HIGH RESOLUTION DIGITAL ELEVATION MODELS OF MARS FROM MOC NARROW ANGLE STEREOIMAGES. R. L. Kirk, E. Howington-Kraus, and B. A. Archinal, U.S. Geological Survey, Flagstaff, AZ (rkirk@usgs.gov).

Introduction: In this abstract we report on our initial experiences performing stereotopographic mapping of Mars with high-resolution images from the Mars Global Surveyor Mars Orbiter Camera Narrow-Angle subsystem (MGS MOC-NA; [1]). Accurate topographic information, and, in particular, high-resolution digital elevation models (DEMs) are of intense interest at all phases of Mars exploration and scientific investigation, from landing site selection to the quantitative analysis of the morphologic record of surface processes. Unfortunately, the availability of extremely high resolution topographic data has hitherto been limited. The current "gold standard" for martian topographic data, the Mars Orbiter Laser Altimeter (MOLA; [2]) has collected data globally with astonishingly high accuracy, but the resolution of this dataset is only about 300 m along track and, in many places near the equator, adjacent MOLA ground tracks are separated by gaps of one to several kilometers. Viking Orbiter images provide stereo coverage of the entire planet at low resolution and expected vertical precision (EP, a function of image resolution and stereo viewing geometry) but highest resolution stereo coverage only of limited areas [3]. Given that the minimum separation of independent stereo measurements is about 3 pixels because of the necessity of matching finite-sized image patches, the highest resolution Viking images, at about 8 m/pixel, support stereomapping only at horizontal resolutions >24 m. Photoclinometry, or shape-from-shading [4] can be used to produce DEMs at the pixel resolution from single images but the results depend on the accuracy of atmospheric and surface radiative transfer models [5]. Calibration of photoclinometry against MOLA data [6,7] promises to reduce uncertainties about the inferred scale of relief, but albedo variations can still lead to artifacts in the resulting DEMs.

The MOC-NA camera, with a maximum resolution of 1.5 m/pixel [1], offers the prospect of stereotopographic mapping at a horizontal resolution of ~5 m and EP ~ 1 m. MOC-NA stereo coverage is limited because most images are obtained with nadir pointing and are not targeted to overlap one another, but at least tens of MOC-MOC stereopairs do exist and further stereo imaging of Mars Exploration Rover (MER) candidate landing sites is an objective of the MGS extended mission. It is also likely that some MOC images will provide useful stereo coverage when paired with oblique Viking Orbiter images. A capability for stereomapping with the MOC-NA images is therefore highly desirable, but the pushbroom scanner geometry of the camera means that new software is required, as that developed for framing cameras, like those of the Viking Orbiter, will not suffice. The other main challenges in working with MOC-NA data are identifying suitable stereopairs and providing adequate geodetic control for such high resolution images.

Software Implementation: The software packages, specialized hardware, and workflow for the MOC mapping reported here are the same as those we use for stereoanalysis of a wide range of planetary datasets ([8]; see also reports [9,10,11] in this conference). We use the USGS in-house digital cartographic software ISIS [12,13,14] for mission-specific data ingestion and calibration steps, as well as "two-dimensional" processing such as map-projection and image mosaicking. Our commercial digital photogrammetric workstation, an LH Systems DPW-790 running SOCET SET software [15,16] includes special hardware for stereo display of images and graphics, and is used mainly for such "three-dimensional" processing steps as automatic and manual measurement of image tiepoints; bundle-block adjustment of image orientations to conform to geodetic control; and automatic extraction and manual editing of DEMs. The ability to view DEM data as graphics overlaid on the images in stereo in order to detect and interactively edit errors is the single most important reason for using the commercial system.

In order to work with planetary data, we have written a set of translator programs drawing on both ISIS and the SOCET SET Developer's Toolkit (DEVKIT) to import images and geometric metadata from ISIS into SOCET SET and export DEMs and orthoimage maps back to ISIS. Images from planetary framing cameras (e.g., Viking, Clementine) can then be analyzed with the framing camera sensor model software supplied as a basic part of SOCET SET. (A sensor model consists of software that carries out the transformation between image and ground coordinates and vice versa, plus a variety of housekeeping routines.) The DEVKIT lets us implement and install sensor models for other instruments, such as the Magellan synthetic aperture radar [11]. After beginning a similar in-house development of a sensor model for the MOC camera, we were able to take a substantial "shortcut" by making use of the generic pushbroom scanner model included in SOCET SET and writing only the software needed to import MOC images and set them up for use with this model.

The generic scanner model computes a physically realistic description of the process by which a scanner image is built up. It is "generic" in the sense that the following parameters must be specified and can be different for different cameras and/or images from the same camera:

- Image size; relation between line number and time
- Camera focal length and lens distortion polynomial
- Camera trajectory in the form of position and velocity at a series of equally spaced times spanning acquisition of the image, to be interpolated
- Camera orientation relative to the vertical and flight direction (nominally assumed constant)
- Corrections to the trajectory and orientation, normally initialized as zero and estimated as part of the bundle-adjustment process
  - Position and velocity offsets in the along-track, across-track, and vertical directions
  - Angular offsets around three orthogonal axes, angular velocities, and angular accelerations

These parameters suffice to describe not only the MOC-NA, but also the wide-angle (WA) cameras, which have been used to obtain global stereo coverage with 240-m resolution [17]; the Mars Express High Resolution Stereo Camera (HRSC) with multiple detector lines for single-pass stereo imaging at 10 m/pixel [18]; and the ultrahigh resolution scanner that NASA has solicited proposals for the Mars Reconnaissance Orbiter mission. Not only can the generic scanner model be used with images from any of these cameras, SOCET SET permits bundle-adjustment and stereo DEM collection with any combination of scanner and framing camera data in a single project. To date, we have written software to collect the necessary information from both MOC-NA and WA image labels, convert geometric quantities from the inertial coordinate system used by ISIS to the local Cartesian system used by SOCET SET, and write this supporting data in the needed format.

The main limitation of the software that affects its use with MOC-NA images is the nominally constant orientation of the camera. Images obtained (during the aerobraking phase of the MGS mission) by rotating the spacecraft do not fit this model, and our experiments with representing the spacecraft rotation by using the adjustable parameters have so far been unsuccessful. An enhancement of the sensor model promised for a future release will allow an arbitrary time history of camera orientation to be specified. The limited set of adjustable parameters in the model also has its drawbacks, and this is unlikely to be changed. The low-order (smooth) position and pointing corrections possible with these parameters cannot address the high-frequency undulations of the MGS spacecraft that are evident in some MOC stereopairs. Nor does the SOCET SET bundle-adjustment software understand that images from a multiline scanner such as HRSC come from the same spacecraft and are subject to the same position and pointing corrections as a function of time. To address these shortcomings it is necessary to implement more capable bundle-adjustment software outside SOCET SET and then import the corrected geometric data derived with such software. We have proposed to NASA to add pushbroom scanner capability to the RAND bundle-adjustment software recently taken over by the USGS. We would initially model single-line scanners, including high-frequency pointing oscillations. Modeling of multiline scanners could be undertaken at a later date if adequate orientation data and/or adjustment software to produce such data are not produced within the Mars Express mission.

Identification of Stereoimagery: Identifying suitable pairs of MOC-NA images for stereoanalysis is a significant challenge, given that more than 30,000 images have been released to date but the typical such image covers only about one millionth of Mars's surface area. We have pursued several approaches to identifying pairs for initial testing of our software. First, MOC press releases on the Malin Space Science Systems (MSSS) website http://www.msss.com/mars_images/moc/MENUS/moc_by_date.html include a number of anaglyphs made from NA stereopairs. Unfortunately, the most dramatic of these stereo views are also the most recent (press releases MOC2-256, 282, 283, and 287) and contain images not yet released. Earlier releases (Table 1) show the Viking 1 (MOC2-44), Mars Polar Lander (MOC2-255), and Mars Pathfinder (MOC2-46; Figure 1) landing sites.

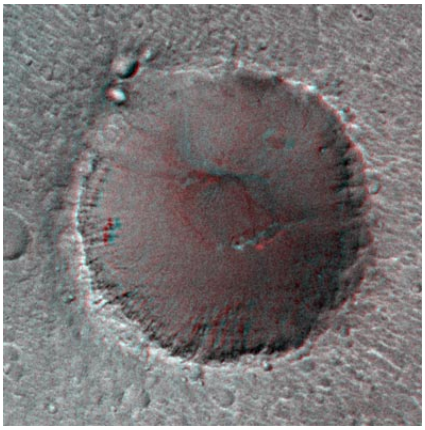

Figure 1. Anaglyph of Big Crater (1.5 km in diameter, located 2.2 km SSE of Mars Pathfinder landing point), taken from MSSS press release MOC2-46. Figure shows a small part of stereo overlap of images and SP1-23703SP1-25603, which extends to Sand W (Fig. 2) but unfortunately does not cover Pathfinder site. For correct stereo impression, view with red filter on right eye.

Of these, the last was selected for initial testing because we have previously mapped parts of the region with both Viking Orbiter [19] and Mars Pathfinder IMP [20] images. The stereo pair unfortunately does not cover the actual landing point, but does include Big Crater (prominent in the lander images) and plains to the south and west. Non-stereo MOC coverage of the landing point shows that it and the plains south of Big Crater are extremely similar in texture and features.

Maps of MOC-NA image coverage of prospective MER landing sites (http://marsoweb.nas.nasa.gov/landingsites/mer2003/mer2003_NS.html) provide another resource for locating stereopairs. Pairs of images that appear to overlap in the footprint plots must be screened to determine if they actually overlap, if they have useful stereo geometry (at a minimum, at least one off-nadir image), and if the illumination is consistent enough between images to permit automatic stereomatching. Applying these criteria by a manual search turned up one additional stereo set not located by other means (Table 1). Unfortunately, the oblique image AB1-07704, which crosses nadir images M08-01457 and M09-01839 in the Hematite area, was obtained with the spacecraft rotating, and our attempts to model this image with the current software have been unsuccessful.

The optimal way to identify stereopairs is obviously through an exhaustive, automated search of catalog data. We previously conducted such a search for the ~45,000 Viking Orbiter images, which yielded ~360,000 potential pairs (i.e., each image overlaps about 8 others), only a fraction of which had useful EP [3]. Here, we report on a similar search of the MOC-NA catalog, based on data taken from the cumindex.tab file on the official MOC releases, plus similar data for pre-released, extended-mission images of the MER landing sites. This search must be considered preliminary, as the criteria used for automatically determining intersection of images were approximate: a test was made whether any of the corners of the minimum bounding rectangle (MBR) of one image in latitude and longitude fell inside the MBR of the other image. This test generated 4,872 candidate pairs from the list of 31,901 images. This list of candidate pairs was narrowed by excluding those with stereo convergence angles too large or too small, and those with dissimilar illumination (criteria similar to those used in [3] and adopted from the work of Cook et al. [21]). This step yielded 158 candidate pairs, 18 of which were located near current MER candidate landing sites. We then examined the pairs at landing sites and eliminated those with little or no overlap, and those with low image contrast due to atmospheric opacity. The resulting list of 9 images forming 5 pairs at 4 sites is shown in Table 2. Properties of the respective stereopairs such as attainable ground sample distance and vertical precision (GSD and EP) are summarized in Table 3. It is noteworthy that all of these images were obtained by 2x2 summation of pixels, so that their resolutions are not as high as the MOC-NA camera is capable of. In all cases, however, the resolutions are better than the best Viking Orbiter images.

We plan in the near future to repeat the search for MOC image pairs, incorporating a rigorous test for the overlap of the actual image footprints (not their MBRs) and using footprints calculated from the mission SPICE kernels (rather than from the cumulative index) to reduce positional errors. Because coordinate errors cannot be eliminated entirely, this search will probably still require a final, manual step of checking the images for their actual overlap and contrast, and it may be useful to "pad" the image footprints by an amount corresponding to the coordinate errors in order to search for images that overlap in fact but not according to their SPICE data. We will also look for mixed pairs of MOC and Viking images that yield usable stereo. In the meantime, we are collecting DEM data from the image pairs described in Tables 2 and 3 in order to produce surface roughness data to support the MER landing site selection process.

Geodetic Control: Our experience with map-projecting and comparing MOC-NA and WA images indicates that errors of position (combining both spacecraft position and pointing errors) are often <100 m but occasionally greater, especially for off-nadir images. This is adequate to produce uncontrolled mosaics of WA images (≥240 m/pixel resolution) but inadequate for the higher resolution NA data. In particular, 100-m relative horizontal errors between images of a stereopair will give rise to comparable vertical errors in the DEM. It is therefore highly desirable to use a bundle-adjustment process to bring the images into consistency with external control. This process is made challenging by the large gap in resolution between the NA images and the next-best datasets available for control. The MOLA dataset, with estimated absolute accuracies of <10 m vertically and ~100 m horizontally [22], is the ultimate source of control, but the spacing of MOLA footprints is hundreds to thousands of MOC-NA pixels. Direct comparison of the MOC images with MOLA profiles or gridded MOLA data is therefore helpful in bringing the stereomodels into vertical correspondence with the altimetry but not very useful for improving their horizontal positioning. In our opinion, the best approach to refining the horizontal position of MOC-NA images and stereomodels would be to tie other images of intermediate resolution (at the moment, this necessarily means Viking Orbiter

images; the best available resolution at each of the MER sites is indicated in Table 2) to the MOLA data and then tie the MOC images to these. This is essentially our approach to stereomapping with Viking images [9] but we have yet to test it with MOC data. The use of a large number of ties between intermediate-resolution images and MOC-NA will be essential to modeling and correcting the high-frequency oscillations of the MGS spacecraft with the advanced bundle-adjustment software we plan to develop. As discussed above, the bundle-adjustment capability currently available as part of SOCET SET does not include modeling of such high-frequency oscillations.

For the purposes of landing site selection, precise relative topographic data (from which slope estimates can be made) is more important than absolute accuracy. Our efforts to control the images listed in Tables 1-2 have therefore focused on bringing the stereomodels into vertical agreement with MOLA data and not on improving horizontal positioning. For each stereopair, we select a well-distributed set of points (typically 10–20) whose locations can be measured on both MOC images. We then assign each point the elevation interpolated from MOLA data at its *a priori* horizontal location. These heights are used as constraints in the bundle-adjustment process, but no constraints are placed on horizontal positions. The form of the MOLA data used in our control process is an in-house USGS product, gridded at 500-m ground sample distance and adjusted to conform to the most recent set of Mars cartographic constants recommended by the International Astronomical Union and International Association of Geodesy [23, 24]. Similar products for the candidate MER landing sites are available online at http://webgis.wr.usgs.gov/mer/.

The control process for the stereopair near the Mars Pathfinder landing site was even simpler. Rather than determining an interpolated MOLA elevation for every tiepoint, we estimated the average MOLA elevation for the region of the stereomodel and loosely constrained a subset of tiepoints (away from Big Crater and other obvious relief) to have this elevation. The result is to underestimate any net regional slope of the stereomodel.

Our attempts to control the stereopairs listed in Table 3 have been complicated by transmission errors in one or both of the images. It is a characteristic of the Huffman coding used to compress these high-resolution images that signal degradation between the spacecraft and ground station can cause the loss of blocks of image lines; if the degradation is extensive, it may not be known how many lines were lost. When this happens, the correct acquisition times of the lines below the gap (needed in sensor model calculations) are lost. We are working on semiautomated approaches to reconstructing the image line count from information returned in the images, but for the time being our approach to working with MOC data after a data dropout is strictly empirical. We first compare the corrupted image with an uncorrupted image of the same region, estimate the number of missing lines, and insert this number of blank lines into the gap to approximately restore the image. We then control the image, being careful to place pass-points only in the section below the gap (if the section above the gap is needed for mapping, we treat it as an independent image) and allowing a larger than usual along-track adjustment of the spacecraft position to account for the error in reconstructing the gap size.

Analysis of DEM Data: In this abstract, we describe the results of topographic mapping near the Mars Pathfinder landing site. Mapping and analysis of the MER sites (Tables 2-3) is in progress and will be reported at the conference. Figure 2 shows image SP1-23703, orthorectified, with superimposed contours derived from the stereo DEM. The low relief of this region is readily apparent: from the bottom to the top of Big Crater the total relief is 300 m. The most prominent feature in the unedited DEM, apart from the crater, is an apparent peak ~75 m high and 120 m across the base, located near the middle right of the image. This is not a real topographic feature, but an artifact caused by local failure of the automatic matching algorithm. It is also visible in a perspective

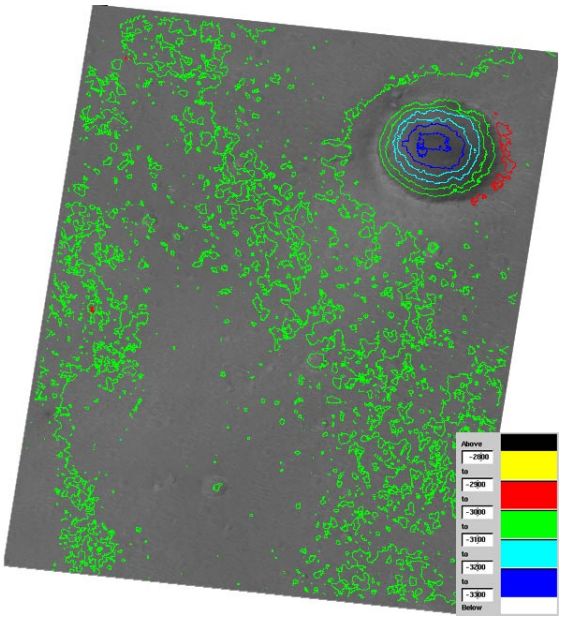

Figure 2. Orthorectified MOC image SP1-23703 with stereo derived contours (contour interval 50 m, color interval 100 m). Total relief from floor to rim of Big Crater is 300 m. Automatic stereomatching was successful except for a single artifact (red dot at center left).

Figure 3. Perspective view of Big Crater from the northwest. 3 m/pixel MOC image SP1-23703 has been draped over 10 m/post stereo-derived DEM. Vertical exaggeration is 2. Matching artifact is visible as a small "hill" in the background. Colors are arbitrary, intended only to suggest the appearance of the martian surface.

view of the DEM (Figure 3). The high overall success of the SOCET SET matcher is gratifying, given the relatively low contrast of the images.

Figure 4 shows the image and DEM data for a portion of the stereomodel excluding both Big Crater and the matching artifact. This section was selected for statistical analysis to characterize the flat part of the landing site. The DEM in this area is consistent with our description based on IMP data of the landing site topography as dominated by ridges and troughs with a

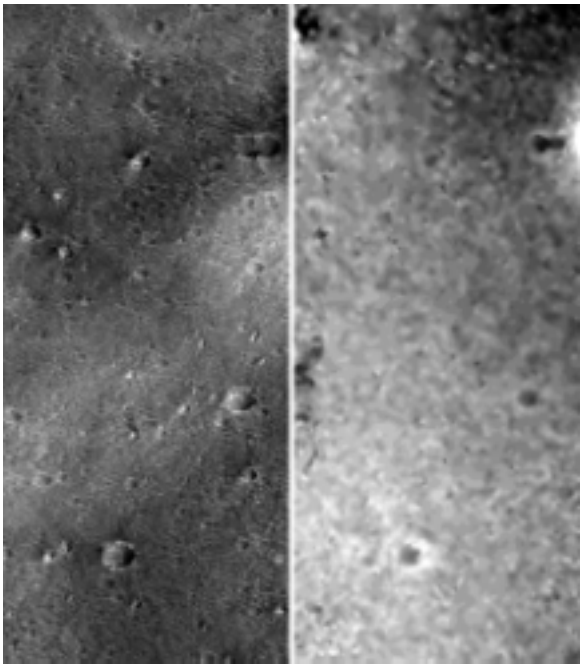

Figure 4. Orthoimage and DEM data (shown at right as grayscale) for ~2.6 x 7.5 km section of the MOC stereomodel SP1-23703/SP1-25603 to the W and S of Big Crater. This region was selected for slope analyses and comparison with results from the Mars Pathfinder lander, which is located on similar plains to the N. Total range of elevations in this area is ≤5 m.

typical amplitude of a few meters and a wavelength of several tens of meters [20]. The smallest ridges are not fully resolved in the DEM but a pattern of somewhat larger ridges can be seen. Comparison of the image and DEM tends to support our previous assertion that many of the bright albedo features in the images are associated with local topographic highs. These are probably strips of light-colored, rock-free sediment similar to those seen (also along ridges) near the lander.

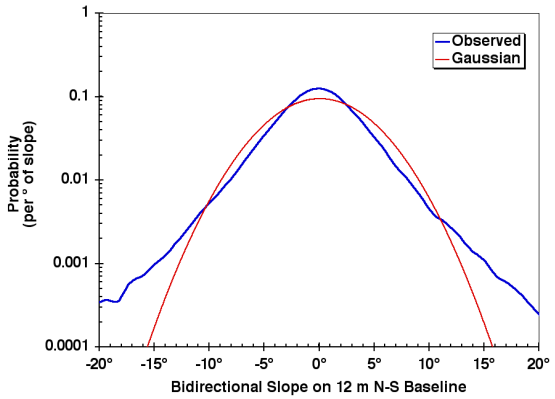

Figure 5. Histogram of bidirectional slopes over a 1-post (12 m) N-S baseline from the portion of the MOC DEM near Big Crater seen in Fig. 4. Gaussian distribution with the same RMS slope (4.2°) as observed is shown for comparison. Large slopes are significantly more common than the Gaussian model would suggest.

Figure 5 shows the distribution of bidirectional slopes derived from the DEM area in Fig. 4, for a north-south baseline of one post (approximately 12 m). The root-mean-squared (RMS) slope is 4.2° but, as the histogram shows, the slope distribution has longer tails (i.e., extreme slopes are relatively more common) than for a Gaussian distribution. Slopes on this baseline are in the range ±14.1° for 99% of the test area. For the adirectional slope (maximum slope in any direction, or gradient) over the same baseline, the 99th % ile is 15.8°.

It is also of interest to look at the RMS slopes over a variety of distance scales. Not only do slopes over long baselines and local slopes have different implications for landing safety and rover trafficability, but this type of analysis lets us compare the MOC DEM with other topographic datasets for the region. If $z(x)$ is a profile of height as a function of horizontal coordinate, and Δ is a horizontal baseline ("lag"), then the one-dimensional autocovariance function $\rho(\Delta)$ is given by

$$\rho(\Delta) = \langle z(x)\, z(x+\Delta) \rangle$$

where the brackets $\langle\ \rangle$ indicate an ensemble average over both x and multiple parallel profiles. From the above definition, it is easy to show that the RMS (dimensionless) slope over the baseline Δ is given by

$$\Theta_{RMS}(\Delta) = \sqrt{\{\, 2\,(\rho(0) - \rho(\Delta)) / \Delta \}}.$$

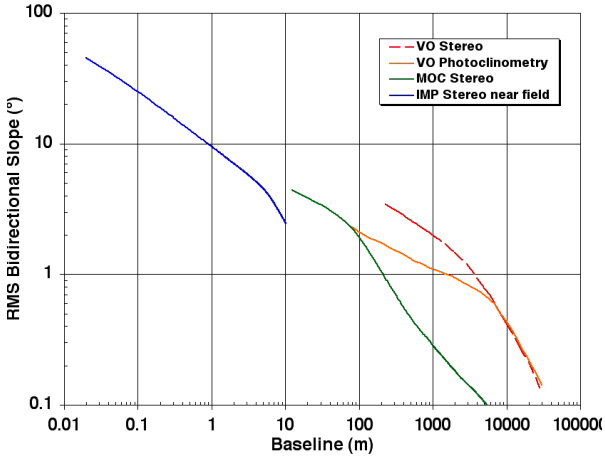

Figure 6. RMS slopes of regions near Mars Pathfinder landing site calculated as described in text from DEMs based on images of a variety of scales and sources. VO stereo DEM covers most of Pathfinder landing ellipse (including some high-relief features) and was interpolated from contours obtained by analytic photogrammetry of 38 m/pixel Viking images [19]. VO photoclinometry dataset was obtained by 2D photoclinometry [4] on 38 m/pixel image 004A72 of smoothest part of landing ellipse after 2x2 pixel averaging; DEM was highpass filtered to suppress artifacts of photoclinometry. MOC stereo DEM derivation is reported here; slope properties were obtained for region shown in Fig. 4. IMP stereo DEM covers region to 10 m from lander at GSD of 2 cm, and was interpolated from data collected on IMP stereopairs with highly variable ground spacing [20]. Slopes over smaller baselines for each DEM are expected to be most accurate and are consistent between datasets. Slopes at longest baselines for each dataset are affected the control process and systematically underestimate real slopes.

Figure 6 is a plot of $\Theta_{RMS}(\Delta)$ calculated from autocovariance estimates obtained by fast Fourier transform techniques for four independent DEMs covering different parts of the Mars Pathfinder landing ellipse at a variety of scales. Dimensionless slopes have been multiplied by the conversion factor from radians to degrees, so the scale is not entirely accurate for the largest slopes. Each of the curves shows a characteristic "dogleg" shape, with a steep section with $\Theta_{RMS}(\Delta) \propto \Delta^{-1}$ for large Δ and a shallower log-log slope at small Δ (the highest resolution dataset does not show an extended steep section but the beginning of a rolloff is nonetheless visible). The steep curves at baselines that are large relative to the respective DEM reflect the fact that each of these topographic models has been controlled essentially to be level overall, so slopes on the longest baselines are underestimated. The "dogleg" in each curve thus reflects the resolution at (and below) which relative topography and slopes are unaffected by errors in control. This scale is especially small (in relation to the DEM size) for our MOC stereomodel because we controlled it to a constant elevation rather than to a realistic distribution of MOLA data.

The continuity of the shallow portions of the Viking photoclinometry, MOC stereo, and IMP stereo curves is striking, given that no two of these datasets cover precisely the same area. The photoclinometry data are taken from Viking image 004A72, which contains only smooth plains similar to those near the lander and south of Big Crater. In contrast, the Viking stereo data cover almost the entire 100x200-km Pathfinder landing ellipse, which contains more rugged features such as craters and streamlined islands [19]. Photoclinometry on images from rougher parts of the landing ellipse yields slope estimates as much as a factor of two greater than for 004A72. The curve for IMP data is derived from a DEM extending 10 m on each side of the lander [20]. Slope estimates over larger baselines can be computed from coarser IMP DEMs extending farther from the lander, but the RMS slope is systematically underestimated in these datasets because much of the distant landing site was hidden behind ridges and the DEMs therefore contain (unrealistically) smooth patches interpolated from actual data for the visible areas. We have therefore not included these estimates in Fig. 6, but their lower RMS slopes are consistent with the value of 4.7° at 1-m baselines quoted in [20].

It is not necessarily the case that the shape of the slope distribution is independent of baseline, but it is likely that this assumption is at least approximately correct over modest baseline variations. If so, the curves in Fig. 6 can also be used to scale estimates of percentile slopes measured at one baseline to a slightly different baseline. For example, if the exponent H - 1 = -0.3 applies to the whole distribution and not just to the RMS slope, then the 99th %ile adirectional slope for the MOC stereo DEM can be extrapolated to a baseline of 5 m, giving a value of 20.4°.

The log-log slope of the curves in Fig. 6 can be interpreted in terms of fractal geometry [25]: if $\Theta_{RMS}(\Delta) \propto \Delta^{H-1}$, where $0 \le H \le 1$ is the Hurst exponent, the fractal dimension of the surface is D = 3 - H. The Viking photoclinometry and MOC stereo datasets show a similar dimension D ~ 2.3, whereas for the IMP data D ~ 2.4. This difference may reflect the structural features (fluvial or eolian ridges vs. rocks) that dominate relief at different scales, but it should be borne in mind that the slope estimates are also affected by the noise properties of the data and method used to produce the DEM. In any case, we find it interesting that a straight-line extrapolation of the Viking photoclinometry curve from baselines ≥80 m yields slopes at centimeter scales that are within a factor of two of those measured *in situ*.

Conclusion: The newly developed software and techniques reported here are opening a door to a new

realm of Mars topography. The ability to produce DEMs with horizontal resolutions of 10 m and better will be invaluable for selecting future landing sites and will contribute greatly to the study of surface processes. These capabilities will be almost immediately applicable to high-resolution stereoimagery from future missions such as Mars Express and Mars Reconnaissance Orbiter, as well.

References: [1] Malin, M. C., et al (1992) Mars Observer Camera, *JGR., 97*, 7699; Malin, M. C., et al. (1998) Early views of the martian surface from the Mars Orbiter Camera of Mars Global Surveyor, *Science, 279,* 1681. [2] Zuber, M. T., et al. (1992) The Mars Observer Laser Altimeter investigation, *JGR, 97*, 7781–7797; Smith, D. E., et al. (1999) The Global Topography of Mars and Implications for Surface Evolution, *Science, 284*, 1495–1503. [3] Kirk, R. L., et al., (1999) A database of Viking Orbiter image coverage for cartographic and scientific use , *LPS XXX*, 1857. [4] Kirk, R. L. (1987), *III. A fast finite-element algorithm for two-dimensional photoclinometry*, Ph.D. Thesis (unpubl.), Caltech. [5] Kirk, R. L., et al., (2001) Photometry of the martian atmosphere: An improved practical model for cartography and photoclinometry, *LPS XXXII*, 1874. [6] Herkenhoff, K. E., et al. (1999) Geologic studies of the Mars Surveyor 1998 landing area, *LPS XXX*, 1120 [7] Soderblom, L. A., et al. (2001) Accurate fine-scale topographic profiles in the martian south polar region from MOLA-Calibrated photometric modeling of MOC NA images, this conference. [8] Kirk, R. L., et al. (2000) Recent planetary topographic mapping at the USGS, Flagstaff: Moon, Mars, Venus, and beyond, *Int. Arch. Photogramm. Remote Sens., XXXIII*(B4)**,** 476 (CD-ROM). [9] Rosiek, M. R., et al. (2001) Utilizing Mars Digital Image Model (MDIM) and Mars Orbiter Laser Altimeter (MOLA) data for photogrammetric control, this conference. [10] Rosiek, M. R., et al. (2001) Combining lunar photogrammetric topographic data with Clementine LIDAR data, this conference. [11] Howington-Kraus, E., et al. (2001) Validation of the USGS sensor model for topographic mapping of Venus using Magellan radar stereoimagery, this conference. [12] Eliason, E. (1997) Production of digital image models using the ISIS system, *LPS XXVIII,* 331-332. [13] Gaddis, L. et al. (1997) An overview of the Integrated Software for Imaging Spectrometers (ISIS), *LPS XXVIII,* 387-388. [14] Torson, J. and Becker, K. (1997) ISIS: A software architecture for processing planetary images, *LPS XXVIII,* 1443-1444.. [15] Miller, S.B. and Walker, A. S. (1993) Further developments of Leica digital photogrammetric systems by Helava, *ACSM/ASPRS Annual Convention and Exposition Technical Papers, 3, 256-263.* [16] Miller, S.B. and Walker, A.S. (1995) Die Entwicklung der digitalen photogrammetrischen Systeme von Leica und Helava, *Z. Photogramm. Fernerkundung, 1/95,* 4-16. [17] Caplinger, M. A., and M. C. Malin (2001) The Mars Orbiter Camera geodesy campaign, *JGR*, in press. [18] Albertz, J., et al. (1992) The camera experiments HRSC and WAOSS on the Mars 94 mission, *Int. Arch. Photogramm. Remote Sens.*, *29*(B1), 130–137. [19] Howington-Kraus, E., et al. (1995) High-resolution topographic map of the Ares-Tiu landing site from Viking Orbiter data. In: Mars Pathfinder Landing Site Workshop II, LPI Tech. Rep. 95-01, 38–39; map reproduced in Tanaka, K. L. (1997) Sedimentary History and Mass Flow Structures of Chryse and Acidalia Planitia, Mars, *JGR, 102*, 4131–4149. [20] Kirk., R. L., et al. (1999) Digital photogrammetric analysis of the IMP camera images: Mapping the Mars Pathfinder landing site in three dimensions. *JGR*, *104*(E4), 8869–8887. [21] Cook, A. C., et al. (1996) Clementine imagery: selenographic coverage for cartographic and scientific use, *Planet. Space Sci*., *44*(10), 1135-1148.. [22] Neumann, G. A., et al. (2001) The crossover analysis of Mars Orbiter Laser Altimeter data, *JGR*, in press. [23] Duxbury et al. (2001) Mars Geodesy/Cartography working Group recommendations on Mars cartographic constants and coordinate systems, this conference. [24] Seidelman P. K., et al. (2001) Report of the IAU/IAG working group on cartographic coordinates and rotational elements of the planets and satellites: 2000, *Celest. Mech. Dyn. Astron.,* in press. [25] Turcotte, D. L. (1997) *Fractals and Chaos in Geology and Geophysics*, Cambridge Univ. Press, New York..

Table 1. MOC Stereo Image Pairs of Landing Sites Found by Manual Search

Site	Image	Lon (°)	Lat (°)	Res (m)	ε (°)	ι (°)	Sun Az (°)	VO Res (m)
Viking 1	SP1-23503	48.30	22.59	2.6	31.4	50.5	53.4	16
	SP1-25403	48.30	22.49	2.5	22.3	54.7	43.9	
Mars Pathfinder	SP1-25603	33.50	19.30	3.2	30.7	56.1	38.0	38
	SP1-23703	33.60	19.20	2.6	21.4	50.9	46.6	
Mars Polar Lander	M11-01286	-76.96	200.15	1.4	0.0	55.1	228.3	130
	M11-01563	-76.65	195.55	1.4	1.3	54.9	228.2	
	M11-03519	-76.67	195.69	1.8	29.7	69.5	246.5	
Hematite (MER)	AB1-07704	5.62	-3.26	11.8	50.1	36.0	144.4	230
	M08-01457	4.94	-70.92	2.8	0.3	61.9	217.5	
	M09-01839	6.02	-1.73	11.5	0.2	39.3	147.0	

Table 2. MOC Stereo Image Pairs of MER Landing Sites Found by Automated Search

Site	Image	Lon (°)	Lat (°)	Res (m)	ε (°)	ι (°)	Sun Az (°)	VO Res (m)
Eos Chasma	E02-02855	41.47	-13.46	4.3	0.2	48.2	216.9	57
	E04-01275	41.50	-13.46	3.3	21.9	47.0	203.4	
Melas Chasma	E02-00270	77.77	-8.87	2.9	0.2	46.8	218.9	68
	E05-01626	77.76	-8.82	3.0	12.8	40.2	200.5	
Gusev Crater	E02-00665	184.06	-14.96	2.9	0.2	50.7	222.1	76
	E02-01453	184.05	-14.87	3.3	22.1	48.3	222.4	
	E03-01511	184.01	-14.96	2.9	0.2	48.0	214.2	
Isidis	E02-01301	275.19	4.64	3.1	13.0	37.4	205.1	53
	E02-02016	275.21	4.66	2.9	0.2	38.6	202.7	

In Tables 1 and 2, Lon and Lat are planetographic/west longitude and latitude, Res is resolution, ε and ι are emission and incidence angles, Sun Az is azimuth of Sun measured clockwise from east, and VO Res is the approximate resoluton of the best available Viking Orbiter images at the given location.

Table 3. Properties of MOC Stereopairs of MER Landing Sites

Site	Image 1	Image 2	Res (m)	GSD (m)	c.a. (°)	EP (m)
Eos Chasma	E02-02855	E04-02855	4.3	13	21.7	2.2
Melas Chasma	E02-00270	E05-01626	2.9	9	12.6	2.7
Gusev Crater	E02-00665	E02-01453	3.3	10	21.9	1.6
	E02-01453	E03-01511	3.3	10	21.9	1.6
Isidis	E02-01301	E02-02016	3.1	9	12.8	2.7

Res is the coarser of the two image resolutions. GSD is minimum achievable ground sample distance for DEM, given as 3 times Res. c.a. is convergence angle. EP is expected vertical precision, equal to 0.2 Res / tan(c.a.).